Optimization of a Single-Particle Micropatterning System With Robotic nDEP-Tweezers

Kaicheng Huang, Zhenxi Cui, Jiewen Lai, *Student Member, IEEE*, Bo Lu, and Henry K. Chu, *Member, IEEE*

***Abstract*— In this study, a system of automatic microparticle patterning that could enable the separation, trapping, and translation of single microbeads in liquid suspension using negative dielectrophoresis (DEP) tweezers was presented to form a single-bead pattern. A microchip with integrated electrodes was flipped and placed above the substrate through a micromanipulator. Microparticles laying on the substrate could be displaced to different positions relative to the electrodes on the microchip, and only the selected particles would be trapped by the electric fields generated from electrodes. Vision-based approaches were used to evaluate the necessary information, such as the gap distance and the positions of electrodes and microparticles in the image. A strategy for separating nearby particles was proposed to achieve single-bead patterning with high accuracy. A controller was used to guide the microparticles toward the position for trapping while avoiding flow disturbance. Different strategies were simulated to decrease the patterning time and find the minimum traveling distance and the best route of movement. The optimization problem is NP-hard. Hence, global optimization algorithms, such as genetic algorithm, particle swarm optimization, and ant colony optimization (ACO), were simulated, and the results were compared with those of the local optimization method. The comparison results showed that ACO obtained the best performance among the methods. The strategy for constructing high-quality microparticle patterns was also examined through experiments. Orange fluorescent polystyrene beads suspended in 6-aminohexanoic acid solution were considered and successfully patterned on a glass substrate by using the proposed system.**

***Note to Practitioners*—Micropatterning is an effective tool for pharmaceutical research and drug discovery. However, the reliability of results depends on the quality of patterns. Existing approaches, such as microfluidic devices, are limited to create a pattern from one chip for single use, and the entire process is sealed and isolated from the environment. In this study, a multielectrode microchip combined with a vision-based micromanipulator is introduced to create a novel noncontact approach for microparticle patterning, which offers high flexibility and guarantees the quality of the constructed patterns. The electrodes on the chip can be selectively energized to determine the shape of the final pattern. A real-time screening is performed so that the micromanipulator will only guide the particles in good condition for selection. An optimization algorithm is implemented to aid the particle selection with the electrodes, allowing high-quality microparticle patterns to be constructed in a short time for various applications.**

***Index Terms*— Automatic control, dielectrophoresis (DEP), micro and nano scales, micromanipulation, micropatterning.**

I. Introduction

MICROPARTICLE patterning plays an important role in the field of biology and pharmacy. In data analytics, scientists successfully achieve fast testing and analysis with the patterning of high-throughput biological particles. Research on rapid immunoassay involves the arrangement of large numbers of antibody structures in an array for testing [1]. Moreover, microparticle patterning combined with different methods has an important contribution to bioanalytics. Zhou *et al.* [2] applied the on-chip microarray with high-content imaging to achieve single-cell analysis. Sims and Allbritton [3] combined polymerase chain reaction with a single-cell patterning chip to analyze mammalian cells rapidly. Kim *et al.* [4] examined the lipid inhibition activity with antiobesity agents by forming mouse embryo fibroblast cells in a pattern. Liu *et al.* [5] used a microfluidic chip with poly(ethylene glycol) microarray to hold the cancer cells in an array for drug testing. Cell patterning is also a key problem needing a solution in tissue engineering. Certain organs have a particular cell arrangement in their function. For instance, hepatic lobule, which is the building block of the liver, has a hexagonal shape with hepatocytes (liver cells) arranged in radial lines between interlobular veins. Hence, to construct an artificial hepatic lobule, the hepatocytes should be seeded radially rather than arbitrarily on a hexagon scaffold.

To achieve microparticle patterning, dielectrophoresis (DEP)-based lab-on-a-chip (LOC) devices are widely used in microparticle manipulation, especially biological particles, such as cells because pretreatments are unnecessary in the target particles. Under a nonuniform electric field, electrically neutral microparticles can be polarized and result in

Manuscript received February 9, 2021; accepted February 15, 2021. Date of publication March 12, 2021; date of current version April 7, 2022. This article was recommended for publication by Associate Editor X. Liu and Editor D. O. Popa upon evaluation of the reviewers' comments. This work was supported in part by the Research Grant Council of the Hong Kong Special Administrative Region, China, under Grant 25204016 and in part by the PolyU Grant UKFR. *(Corresponding author: Henry K. Chu.)*

Kaicheng Huang was with the Department of Mechanical Engineering, The Hong Kong Polytechnic University, Hong Kong. He is now with the Department of Industrial and Manufacturing Systems Engineering, The University of Hong Kong, Hong Kong.

Zhenxi Cui, Jiewen Lai, and Henry K. Chu are with the Department of Mechanical Engineering, The Hong Kong Polytechnic University, Hong Kong (e-mail: henry.chu@polyu.edu.hk).

Bo Lu is with the T Stone Robotics Institute, The Chinese University of Hong Kong, Hong Kong.

Color versions of one or more figures in this article are available at https://doi.org/10.1109/TASE.2021.3062064.

Digital Object Identifier 10.1109/TASE.2021.3062064

the noncontact manipulation by using the induced force [6]. In micropatterning, several groups [7]–[9] developed simple microfluidic devices to create line and dot patterns with cells. Although different micropatterns can be created with this method, the precision and quality of the pattern cannot be guaranteed with the DEP technology because of its open-loop system. The electrodes used in generating electric fields can only be turned on or off without any other control option. Therefore, the flexibility of the DEP technique is very limited.

Research on extending the functionality of the DEP-based microfluidic devices is known as light-induced DEP. Light beams are used to induce electric fields from a pair of photosensitive semiconductors rather than those from fixed metal electrodes. The location of focused light beams can be changed to adjust the induced electric field inside the microfluidic device and facilitate the transport of microparticles. Through the creation of different light patterns, multiple particles can be manipulated simultaneously for various functions, such as cell sorting [10], storing [11], and forming different microparticle patterns [12]. This technique can be applied to both nonbiological particle [13] and biological cell [14]–[16].

Similar to light-induced DEP, the use of optical tweezers is a micromanipulation technique that relies on the utilization of robotic-aided light beams in the creation and manipulation of optical traps, which can manipulate the microparticles without physical contact. Microparticles, such as biological cells, biomolecules, and polystyrenes (PS) beads, can all be manipulated with optical tweezers [17]–[20]. To manipulate a microparticle precisely in a noncontact manner, the motion control of a particle through optical tweezers is widely investigated. Chowdhury *et al.* [18] derived a simplified dynamic model for translation and rotation control of a biological cell through optical tweezers, and experiments were performed to demonstrate the effectiveness of the model. Ju *et al.* [21] considered using a rapidly exploring random tree algorithm to generate an appropriate path for cell translation with optical tweezers to address the disturbance problem in dynamic solutions. Yang *et al.* [22] performed translation for a group of cells during the cell surgery, and cells were kept in a group while avoiding collisions. Li *et al.* [23] elaborated the dynamic cell model and combined with the dynamics of a robot manipulator so that the precision during manipulation can be further enhanced. Different controllers were designed to resolve different challenges, such as liquid with high Reynolds number [24], uncertain trapping stiffness [25], and small disturbance [26].

In this study, a low-cost print circuit board (PCB) microchip was used as multiple nDEP-tweezers to generate numerous electric fields for the simultaneous trapping and manipulation of microparticles. Given the economical manner of fabricating the microchip, the electrode design in the microchip can be changed easily to facilitate the requirement. Compared with conventional microfluidic DEP devices, precise control can also be realized with the help of a 3D movement platform in an open environment. In the previous work, a microchip with a 4×4 dot electrode array was designed and used to create different cell patterns. By selectively energizing any of the 16 ring-like electrodes, the cells were clustered underneath each energized electrode to form different patterns on a glass substrate via DEP [27]. The microchip was inversely mounted on a sliding rail, and the substrate on the motorized stage can be arbitrarily moved with respect to the microchip to ensure that large patterns can be constructed with the cell clusters [28]. Given that the electrodes do not require patterning on the substrate, they can offer high flexibility in the patterning of cell clusters on any kind of biocompatible material substrate [29]. In this study, the system was modified for use in the creation of patterns with single-beads only. Given that the process involves the selection and control of microbeads, an optimization scheme was incorporated to construct high-quality single-bead patterns efficiently. Micro PS beads with fluorescent colors were considered to conduct experiments. The beads were randomly suspended in an aqueous medium. The electric fields were generated from the electrodes to trap and dispense the selected bead on a glass substrate and form a microbead pattern.

This article is organized as follows. The setup of the entire robotic system and materials used in the experiments is provided in Section II. The vision-based algorithms in this automated system and experimental protocols in single-bead trapping and patterning are described in Section III. The steps in implementing global optimization methods for use with the patterning system and three global optimization algorithms (ant colony optimization [ACO], particle swarm optimization [PSO], and genetic algorithm [GA]) are discussed in Section IV. The results and discussion of the system performance are presented in Section V. Finally, a summary is given at the end of this article.

II. System Setup

A. Principle of DEP

The main component of the system is a multilayer microchip that uses the DEP technique to create nonuniform electric fields through the electrodes located at the different layers for microparticle manipulation and trapping [27]. The results in Pohl [6] indicating that all particles could be polarized in a spatially nonuniform electric field. The dipole induced in the particle leads to a net DEP force that drives the particle in a nonuniform electric field environment. The force acting on a spherical microparticle, $\boldsymbol{F}_{\mathrm{DEP}}$ can be evaluated as follows:

$$\boldsymbol{F}_{\mathrm{DEP}} = 2\pi r^3 \varepsilon_m \cdot \mathrm{Re}[K(\omega)] \cdot \bigtriangledown E^2 \tag{1}$$

where r is the radius of the particle, ε_m is the permittivity of the suspending medium, $\bigtriangledown$ is the Del vector operator, E is the gradient of the electric field, and $\mathrm{Re}[K(\omega)]$ is the real part of the Clausius–Mossotti factor that can be calculated as follows:

$$K(\omega) = \frac{\varepsilon_p^* - \varepsilon_m^*}{\varepsilon_p^* + 2\varepsilon_m^*} \tag{2}$$

where ε_p^* and ε_m^* are the complex permittivity of the particle and suspension medium, respectively. According to (1), the strength of the DEP force is proportional to the gradient of the electric field, which is related to the input voltage and the particle position with respect to the electrode. Therefore, increasing the voltage or reducing the gap between

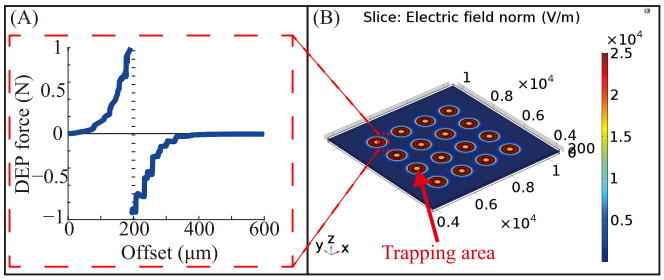

Fig. 1. (a) Normalized DEP force versus position. (b) Electric field simulation of the microchip.

the electrode and the substrate can help improve the DEP force acting on the particles for manipulation.

The direction of the force acting on the particle is dependent on the gradient of the electric field and relative polarizability between the particle and the medium. The relative polarizability is based on the electrical properties of the medium and particle (conductivity and relative permittivity). The phenomenon of particles moving from the weak electric field toward the strong part is called positive DEP (p-DEP), whereas moving in the opposite direction is referred to as negative DEP (n-DEP). Given that the microchip is inversely held against the substrate, the n-DEP force is required to drive the beads toward the substrate underneath the electrodes to arrange and pattern the beads onto the substrate. On the basis of the experimental results in our previous study [30], the signal frequency in this work was set at above 8 MHz to induce the n-DEP force in the PS beads while avoiding electrolysis.

B. Design of the Micropatterning System

The microchip design can effectively generate ring-like electric fields within the microenvironment to drive the surrounding microparticles toward the center of each electrode and subsequently form patterns onto the substrate in our previous study [27]. It consists of 16 circle-surrounding electrode pairs which were fabricated using the conventional PCB technique. However, a single microchip is still unavailable for precise micropatterning. A robotic-aided method is introduced to resolve this problem and ensure that controllers can be applied to the microchip. Several key modifications were made to the system in this study. First, the spacing between electrodes in the microchip was set to 700 μm to prevent possible interference from nearby electrodes. The electric field simulation of the new microchip is shown in Fig. 1(b). A large spacing guaranteed the movement of microbeads between electrodes. The microchip was mounted on a 3-DOF micromanipulator through a chip holder, which is fabricated with a bending rod and the 3-D printed part to provide precise alignment between the microchip and substrate surface. A vision-based algorithm was applied to the system for the precise positioning of the microchip at 200 μm above the substrate by monitoring the image sharpness. The correlated movement between the microbeads and microchip was induced by the motorized platform of the microscope to maintain the microchip within the region of interest (ROI). Moreover, the platform position could be controlled by using a computer. The microscope system Leica DMi8 model was used for inspection. A glass substrate was placed on the motorized platform stage in the microscope system to position the glass substrate underneath the microchip for bead translation. A motorized vertical stage was used to adjust the objective lens. To control the ON–OFF switching of individual electrodes for the selective trapping of microbeads, the relay controlled by the Arduino board was used to energize the electrodes and induce the electric field. A control interface was developed using the C++ program, which can display images from the microscope to facilitate the coordinated movements between the micromanipulator, motorized platform, and vertical stage. The complete setup of the automatic bead patterning system is shown in Fig. 2.

A separation method was developed to achieve single-bead patterning and manipulate the targeted bead toward the desired position with respect to the electrode such that the nearby beads could be repelled by the electric field. To avoid the local electric field minima of other electrodes from influencing the target bead, path planning was incorporated for bead manipulation. A PID controller was applied to the system to guide the target bead in following the planned path. To avoid finding the local minima in the optimization process of selecting the beads for trapping, global optimization methods were considered, and their performance was analyzed through simulation. A series of simulations and experiments was performed to examine the effectiveness of the separation method, patterning strategy, and bead positioning with control algorithm. To test the robustness of the system, two different PS beads (40 μm in diameter with orange fluorescent and 125 μm in diameter with green fluorescent) were used in the patterning experiments.

C. Materials in the Experiments

PS beads were considered to create different patterns on the glass substrate. During the experiments, the microbeads that gradually sunk to the bottom due to gravity resulted in a strong adhesion force that resisted movement. To minimize the effect, 6-aminohexanoic acid (AHA) solution was used as it provides a higher buoyancy force than deionized (DI) water while maintaining low conductivity and avoiding the phenomenon of electrolysis [28]. Given that PS beads have a density of 1.05 g/cm^3, the AHA solution was adjusted to 2.8M to increase the density ($\rho = 1.0798$ g/cm^3). The bead concentration is one of the important factors as it controls the ratio between the beads and the electrodes in the current view for patterning. If the concentration is too high, the distance between beads would be decreased and many of the beads could not be selected for patterning. In this study, the concentration of PS beads in the solution was set to 0.02%w/v.

Furthermore, changing the properties of the substrate also helped decrease the adhesion force [28]. As the glass slides were used as the substrate for bead patterning, the glass substrate was treated in an expanded plasma cleaner (Harrick Plasma, USA) for 10 s prior to experiments to induce polar functional groups and change the surface property from hydrophobic to hydrophilic.

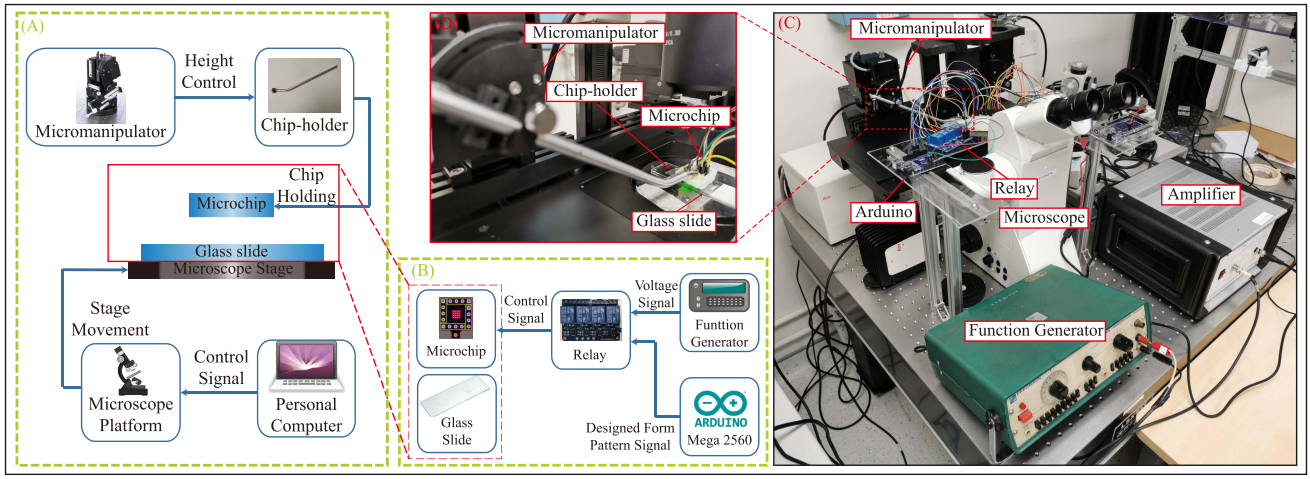

Fig. 2. Diagram of the system setup. (a) Components of the system mechanical setup. (b) Components for generating the selected output signals. (c) Real image of the experimental setup. (d) Enlarged view of the working area.

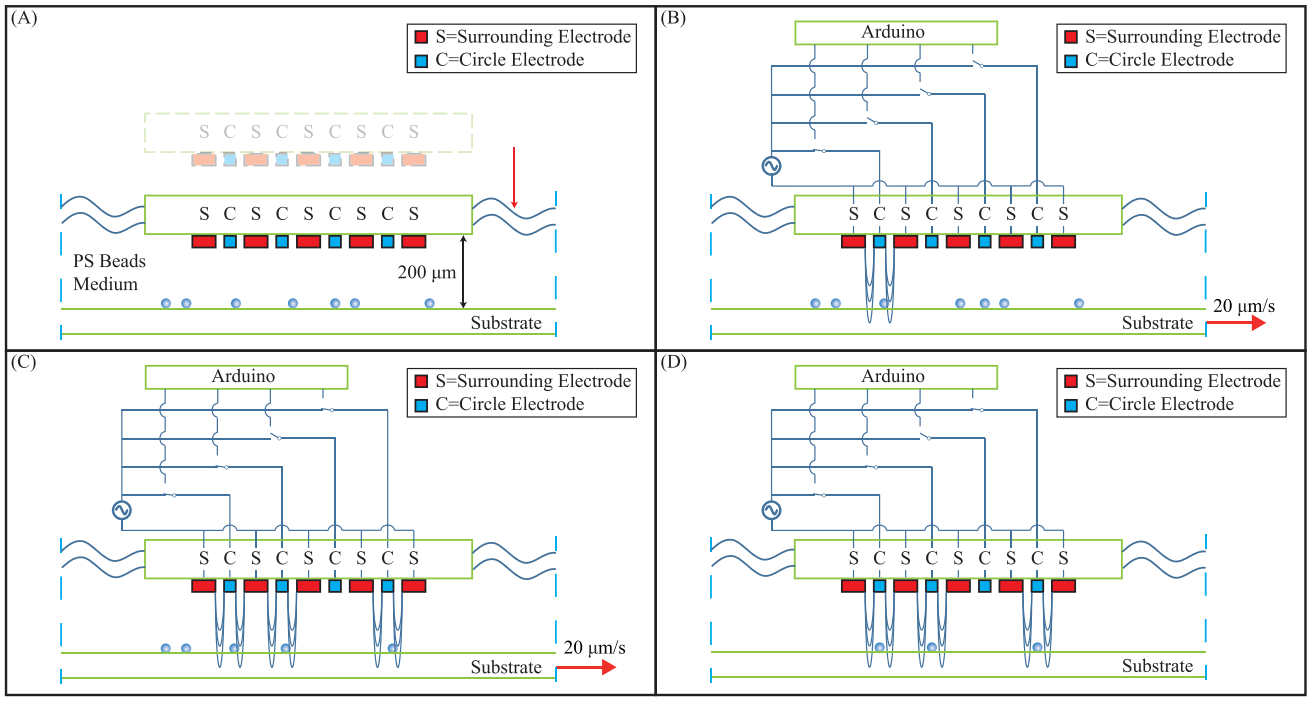

Fig. 3. Microbead patterning procedure. (a) Microbead solution is placed on the substrate, and the microchip is moved down to the substrate with a 200-μm gap. (b) Substrate is moved by the platform to transfer beads beneath electrodes, and the individual electrode pairs are then energized to hold the beads. (c) Substrate is continuously moved by the platform until all the selected electrodes have with beads. (d) Substrate is finally moved such that the patterned beads are transferred to the clean area without other redundant beads.

III. Experiment Protocol

The PS beads in the AHA solution were used, and a droplet of the solution was dispensed on the substrate. The microchip was lowered to be immersed in the medium at 200 μm above the substrate [see Fig. 3(a)]. The height of the microchip was precisely controlled through visual feedback. A detection program was used to obtain the relative positions and shape of electrodes and PS beads within the field. Global optimization was applied to the position information to compute the optimal strategy for trapping the microbeads. Through the movable stage and at a speed of 20 μm/s, the microbeads were manipulated toward the bottom of each electrode for trapping. Depending on the pattern, the electrodes on the microchip could selectively be energized and turned on to hold the microbeads [see Fig. 3(b) and (c)]. Tracking control was applied to the stage to ensure that the microbeads would follow the planned path. After bead trapping, the microchip with the microbead pattern was transferred to a clean region, and the electrodes were deenergized to release the beads onto the substrate [see Fig. 3(d)].

A. Microchip Positioning With Focus Measure Function

The experiment required the microchip to be located at 200 μm above the glass substrate. Therefore, an image-based

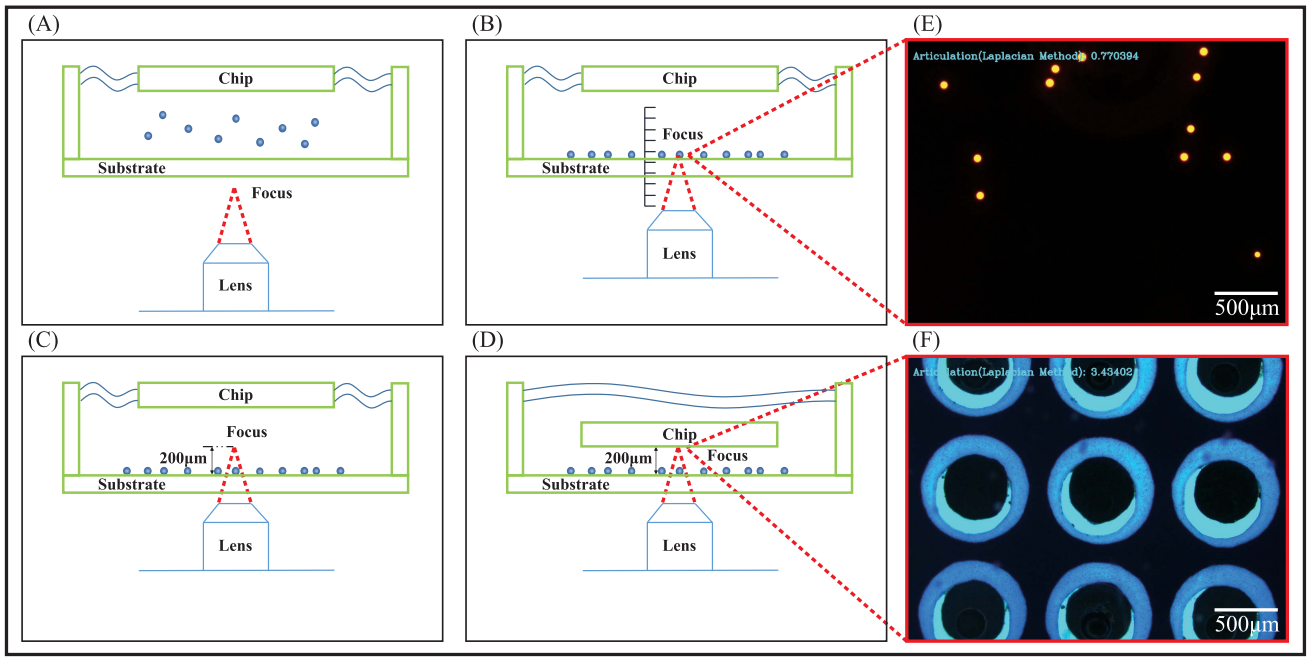

Fig. 4. Microchip setting procedure. (a) Microchip is immersed in the solution from a higher place, while the lens is focused lower than the surface of substrate, wait for the microbeads to sink. (b) Lens is then moved upward with a small increment each time to focus on the surface with beads in a high value of sharpness. (c) After locating the position of microbeads, lens is moved upward with a 200-μm distance. (d) Microchip is continuously lowered until the image sharpness reaches the maximum. (e) Focused image of the microbeads. (f) Focused image of the microchip.

method was used for height evaluation, as shown in Fig. 4. First, the objective lens was adjusted to focus on the surface of the glass slide [see Fig. 4(a) and (b)], in which the microscope image could show the beads adhering to the surface in focus [see Fig. 4(e)]. Second, the objective lens was repositioned to focus at 200 μm above the glass substrate [see Fig. 4(c)]. The micromanipulator was adjusted to move the microchip toward the substrate surface [see Fig. 4(d)]. By continuously monitoring the microscope images, the micromanipulator would stop until the microchip in the image was in focus [see Fig. 4(f)]. To determine whether the image was in focus, the sharpness evaluation method was used to detect the image.

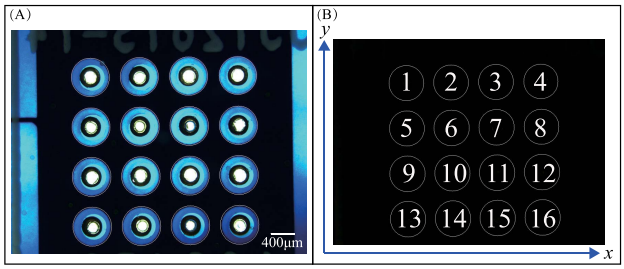

Fig. 5. Images of the microchip under the microscope using (a) transmitted light and (b) reflected light with electrodes labeled by the program with white circles.

B. Detection of the Microchip Electrodes and PS Beads

Given that the system needed to transfer the PS beads to the bottom of the electrode for trapping, a program was developed to detect the position of the electrodes and all the beads presented in the image. During the experiments, fluorescence images were used to monitor. The PS beads and background are maintained in a dark environment. Since the microchip became invisible in the dark, the bright-field images were overlaid to aid the detection of electrode positions. The relative position between the electrode and the PS beads could be determined with this information.

To evaluate the positions of electrodes, the color images from the microscope were first converted into grayscale and then turned into binary for image processing. The fine details were smoothened using the Gaussian filter, and the image noises were removed via morphological operations. With the limited field of view of the microscope, certain electrodes may only be partially captured, as shown in Fig. 5(a). To separate the electrodes from the background, the pixels in the image were grouped into multiple regions. The largest region, which belongs to the common electrode, was neglected and the remaining regions were labeled accordingly as electrodes 1–9. To evaluate the topological information of these regions, the contours were extracted using the algorithm proposed by Suzuki and Be [31]. This algorithm can predict the entire geometry even if only partial information is provided, and the centers and radii of individual electrodes can be calculated, as shown in Fig. 5(b) (white lines).

C. Patterning Procedure

Individual electrodes were energized to perform single-bead patterning and trapping. The beads were sequentially moved to the bottom of the electrodes. The energizing sequence would follow the number, as shown in Fig. 5(b). The procedure is shown using Fig. 6. First, the position of the electrodes and all beads within the image were located

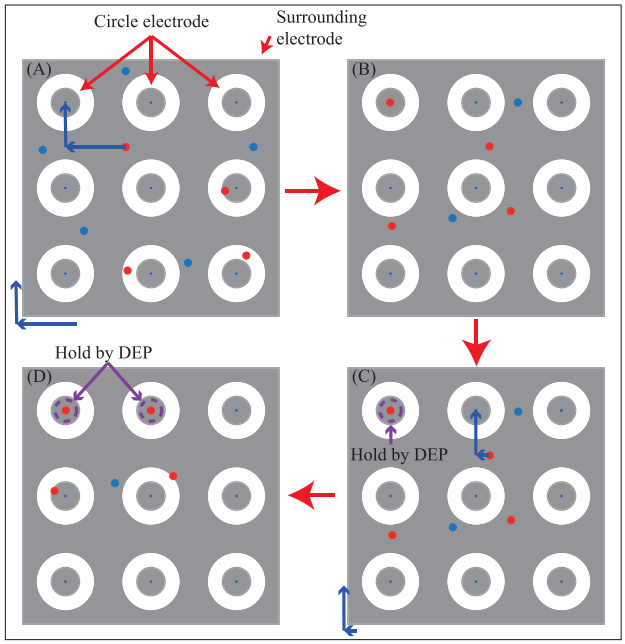

Fig. 6. Procedure of bead patterning. (a) Move the first chosen bead to the first electrode with the microscope platform. (b) Energize the first electrode. (c) Move the second chosen bead to the second electrode. (d) Energize the second electrode.

(small dots in Fig. 6). Second, the bead separation algorithm was employed to find the optimal trapping position for each bead. Any inseparable beads would remain uncounted in patterning. During patterning, all the separable beads and their respective optimal trapping position would be considered to determine the trapping sequence, which could minimize the moving distance. The selected beads for patterning (red dots in Fig. 6) would be trapped and patterned in sequence. Through the motorized platform of the microscope system, the whole substrate was driven and the first chosen bead was manipulated toward the first electrode for trapping [shown in Fig. 6(a)]. The substrate along with other suspending beads was moved together to ensure that the chosen bead was positioned within the electrode [shown in Fig. 6(b)]. The electrode was then energized to hold the bead via the DEP force [see Fig. 6(c)]. The procedure was repeated until all the electrodes were utilized in patterning.

The concentration of PS beads in the solution was highly correlated with the number of beads present in the field. When the concentration was low, the number of beads in the field of view might be insufficient in providing beads for every electrode. In this scenario, the platform would continuously move in the upward direction (image) to search for additional beads and compensate for the remaining electrode. Although this approach might take a long time to complete the patterning process, using high concentrations could help provide additional beads in the selection at the initial state of trapping. However, increasing the concentration would also lead to the likelihood of beads becoming close to one another. Guaranteeing that only one bead would fall within the boundary of the electrode could be difficult and many beads would be counted as inseparable beads and not considered.

D. Bead Separation for Single-Bead Trapping

Ideally, only one bead should be allowed to flow in and be trapped by each electrode. However, as discussed, nearby beads could also be trapped by the same electrode. To avoid this problem, the electric field at the boundary of the electrode could be used for effective bead separation. The relationship between the normalized DEP force and distance to the center of the electrode is shown in Fig. 1(a). This figure shows that the highest electric field occurs at the boundary, and the strength of the electric field decreases while moving away from the boundary. The direction of the DEP force changes significantly from the inner and outer sides of the boundary in an electrode with a radius of the 200 μm, to provide the maximum force for the bead repulsion in opposite direction.

Consider an image with a number of beads presented, as shown in Fig. 7. For each bead, determining all the possible positions that can guarantee single-bead trapping was necessary. First, the position of each bead was evaluated in this algorithm using the binary image. Second, one bead was selected at a time and an ROI of 800×800, which can fit the entire electrode, was drawn to enclose the bead at its center. The image was transformed into a binary image (as shown in step 1 of Fig. 7). The selected bead was converted into the dark (i.e., change from 1 to 0) to avoid interference during convolving. Then, a circle kernel with a radius of 200 μm was used as the template and convolved to the ROI. The convolving operation would give a "1" output only if beads are absent in the circle, and the output image was produced. After the operation, the possible positions for bead separation are presented in Fig. 7 (white area). Such possible positions could be used for placing the electrode center in the optimization algorithm.

To further illustrate the concept, the output image obtained from Fig. 7 was overlaid with the fluorescent image, as shown in Fig. 8(a). The selected target bead was encircled in yellow. Within the white area, an electrode with 200-μm radius could be drawn to enclose the target bead, and no other bead was present for trapping. Different situations of bead separation were also used for illustration. Fig. 8(b) shows the scenario where two possible positions are available for bead separation. Fig. 8(c) presents the importance of finding the white area. If the electrode was placed outside the white area, then the target and nearby beads would likely be trapped by the electrode. If the electrode center was moved to the white area, the two beads could be separated at the boundary. Fig. 8(d) shows the scenario that no possible position can be detected for a selected bead. More than one bead could be captured in the process of trapping this bead. Hence, this bead would be ignored in the optimization algorithm.

E. Single-Bead Patterning With Path Following

When the target bead is guided toward the electrode for trapping, it may enter into the electric field zones generated by other electrodes. The electric field in these zones could repel the bead to other positions. The desired trajectories were set to avoid this interference. To ensure that the bead follows the desired path and reaches the desired position precisely, a PID

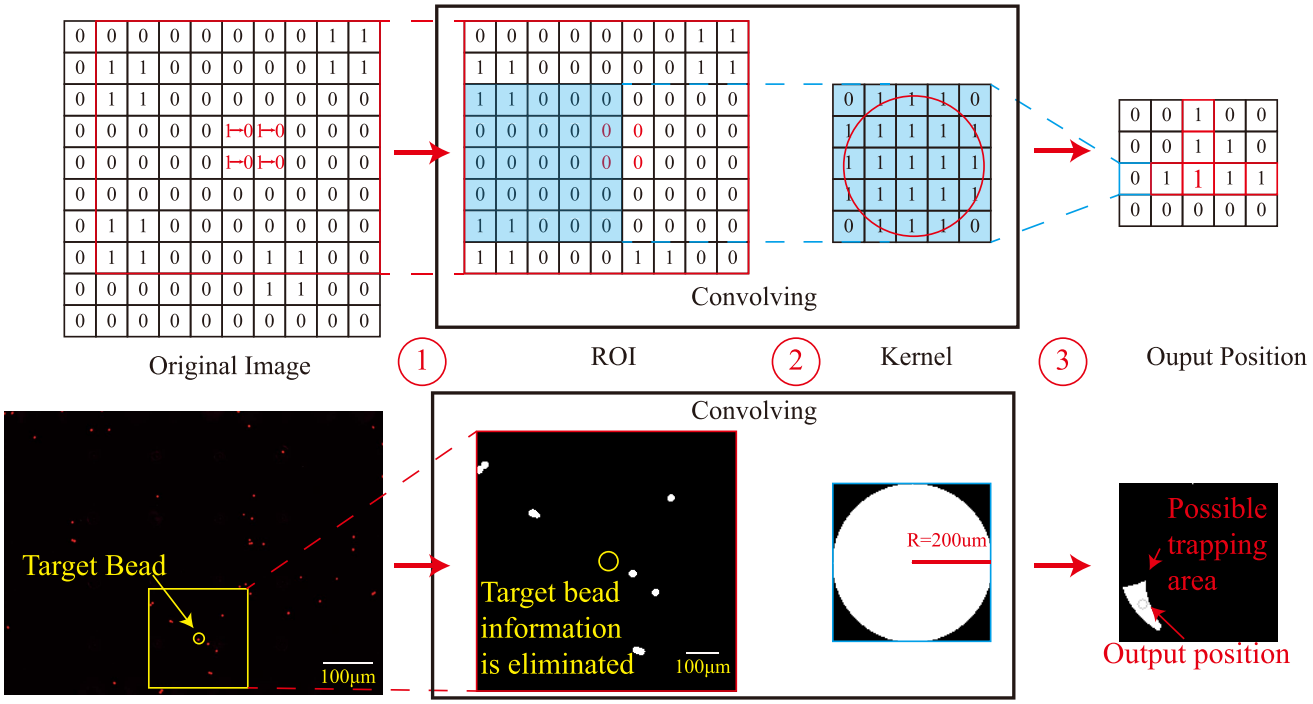

Fig. 7. Procedure for locating the position of single-bead trapping. 1) Extract an ROI around the target bead with a square of 800-μm side. The ROI image is turned into a binary image, while the information of the target bead is eliminated. 2) Convolve the ROI image with a circle kernel (200-μm radius) and negate the result. 3) Locate the center of the output image. The position differences between the output position and the center of the image represent the position difference between the center of the electrode and the position of the target bead, respectively.

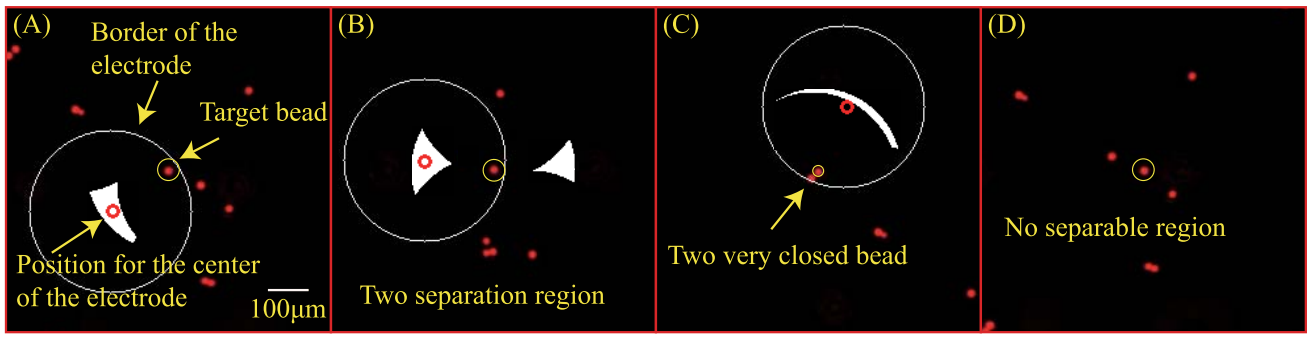

Fig. 8. Results of the bead separation method in different scenarios. (a) Successfully separated result. (b) Configuration with two possible separation trapping regions. (c) Situation with two closed beads. (d) Circumstance of the inseparable bead.

controller was used for path tracking as follows:

$$c(t) = K_p e(t) + K_i \int_0^t e(\tau)\, d\tau + K_p \frac{de(t)}{dt} \tag{3}$$

where $e(t) = x^d(t) - x(t)$ is the position error between the desired tracked bead $x^d(t)$ and the actual tracked bead position $x(t)$. To accelerate the time in evaluating the actual position of the bead in the next step $x(t+1)$, only a small local region was drawn at the current bead position and then used to search for the new bead position. To ensure a satisfactory tracking performance, the bead movement at each time frame was limited to 5 pixels.

During the operation, the energizing of each electrode led to the trapping of beads by certain electrodes during its guidance of another bead to the next electrode. As shown in Fig. 1(a), the effective trapping region was within $x_o = 200$ μm, which was similar to that of optical tweezers [32]. Therefore, an analogous controller must be designed to fulfill the requirement of holding the patterned beads in the trapping zone. The input for the system is expressed as follows:

$$u(t_o) = \begin{cases} c(t_o), & |c| < x_o \quad (4a) \\ x_o, & c \geq x_o \quad (4b) \\ x_o, & -c \leq -x_o. \quad (4c) \end{cases}$$

IV. Patterning Strategy

In contrast to conventional problems that moving multiple beads to multiple traps, the movement through the stage would translate all beads simultaneously (see Fig. 6). In other words, moving one bead to the trap would change the positions of

the remaining beads with respect to the electrodes and the subsequent planning.

In a set of electrodes k and a number of beads n ($k \leq n$), the initial positions of the beads in the field of view are expressed as $p^{[1]} = \{p_1^{[1]}, p_2^{[1]}, \ldots, p_n^{[1]}\}$. The position errors between the particles and electrode 1 were obtained with $e^1 = \{e_1^{[1]}, e_2^{[1]}, \ldots, e_n^{[1]}\}$. After transferring bead i to the bottom of electrode 1, the particle positions in the field of view were determined by using $p^{[2]} = \{p_1^{[2]}, p_2^{[2]}, \ldots, p_n^{[2]}\}$, where $\{p_1^{[2]} = p_1^{[1]} - e_i^{[1]}, \ldots, p_i^{[2]} = p_i^{[1]} - e_i^{[1]}, \ldots, p_n^{[2]} = p_n^{[1]} - e_i^{[1]}\}$. After k steps, all the selected electrodes would be trapped with a bead and the total moving distance of the motorized platform L is

$$L = e_{i_1}^{[1]} + e_{i_2}^{[2]} + \cdots + e_{i_k}^{[k]} \tag{5}$$

where i_k refer to the bead i at the kth step.

A. Distance-First Search (DFS)

The minimum moving distance $L_{\min}$ must be determined to reduce the patterning time. DFS is a simple strategy for finding the beads that are correspondingly nearest to the electrodes. The minimum distance error in each step is calculated as follows:

$$L_{\min} = e_{\min}^1 + e_{\min}^2 + \cdots + e_{\min}^k. \tag{6}$$

At each step, the Euclidean distances between the center of the electrode to be energized and all of the beads in the field were calculated to find the nearest bead. After the bead was transferred to the electrode underneath and trapped, the distance between the next electrode and the remaining beads was updated to find the nearest bead. The procedure was repeated until all selected electrodes were energized.

Given that the position of the particles in step i was evaluated with respect to the previous state $\{p^i = p^{i-1} - e_{\min}^{i-1}\}$, the minimum distance $e_{\min}^i$ in state i would be influenced by the previous movement. Thus, the total moving distance traveled by the platform might not necessarily be the shortest one (global minimum) though the minimum distance could be found in each step (local minimum).

This problem is shown in Fig. 9. In Fig. 9(a), L_1 is slightly larger than L_2. According to DFS, bead 2 was moved first, and the distances from beads 3 and 4 to the center of the next electrode increased from L_3 and L_4 to L_{3A} and L_{4A}. By contrast, if bead 1 was moved first, as shown in Fig. 9(b), then L_3 and L_4 would decrease to L_{3B} and L_{4B}. The total moving distance $L_B = L_1 + L_{3B}$ in the second scenario was smaller than that in the first scenario $L_A = L_2 + L_{4A}$. Therefore, a global optimization algorithm is necessary to find the best patterning sequence. Different global optimization strategies were considered and described in the following.

B. Ant Colony Optimization (ACO)

The ACO algorithm is a multiagent method inspired by the behavior of real ants. Biological ants communicate to encourage the following ants to stay close to the previous moves while laying down pheromone trails for the others. This type of communication helps the ants find the shortest

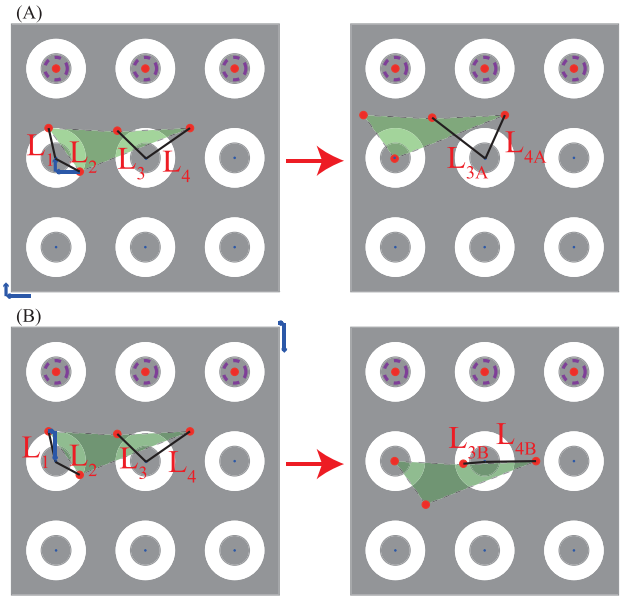

Fig. 9. Problem description with DFS patterning method. (a) Movement of the closest bead will increase the minimum move distance in the next step. (b) Movement of the second closest bead will reduce the minimum move distance in the next step.

path to the food with a feed-forward strategy. In this algorithm, each artificial ant functions as an agent in the system. To apply the algorithm to this work, the microbeads laying on a planar surface are treated as the places with different position coordinates and labeled with an integer number. The artificial ants need to find the shortest route to pass through several of these places depending on the number of electrodes in the microchip. To find the shortest path, artificial ants were arbitrarily placed in one of these places in the beginning. In each iteration, the artificial ants moved to another place on the basis of the old pheromones to create a new pheromone. Once the movement was accomplished, the positions of the places would be updated based on the previous movement. Meanwhile, the previous places for each ant would be recorded and blocked to prevent them from reentering the previous places. After several iterations (depending on the number of electrodes), the best route was recorded and the pheromones were upgraded. A summary of the pseudocode is presented in Algorithm 1. The set of ants m is equal to 500. The elicitation factor (α), heuristic factor (β), and the evaporation coefficient (ρ) are 1, 5, and 0.1, respectively. The maximum number of iterations for the end condition is 20.

C. Particle Swarm Optimization (PSO)

PSO is a computational method that optimizes the entire population of individuals (particles) rather than only on a single individual. Each particle in the swarm was defined with its position and velocity, and the algorithm moved these particles around in a given search space to establish the best outcome. During the iterations, each particle updated its position on the basis of the best position it visited (local best) and the best position among all the particles in the swarm (global best). In this experiment, the PS beads presented in

Algorithm 1 ACO for Bead Trapping Selection

Input: $f(x)$: cost funtion; p_b: position of all beads in field; n_e: number of electrodes; n_b: number of beads;
Output: optimal $x^* \in p_b$

procedure MAIN
  label the beads p_b with integral number
  initial randomly set particle p_{b_1} as the starting point for ant $k \in m$
  repeat
    for $\forall k \in m$ **do**
      for $i = 1$ to n_e **do**
        choose the next particle p_{b_i} with the probability, calculated by the elicitation factor (α), heuristic factor (β), and the evaporation coefficient (ρ);
      end for
    end for
    for $\forall k \in m$ **do**
      calculate the distance L_k though $f(x)$ with the record route;
      record the best route R_{best};
    end for
    for $\forall k \in m$ **do**
      for $i = 1$ to n_e **do**
        update pheromone $\tau_{r,s}$ according to the distance L_k;
      end for
    end for
  until END_CONDITION
end procedure

Algorithm 2 PSO for Bead Trapping Selection

Input: $f(x)$: cost funtion; p_b: position of all beads in field; n_e: number of electrodes; n_b: number of beads;
Output: optimal $x^* \in p_b$

procedure MAIN
  label the beads p_b with integral number
  for each particle $\forall i \in m$ **do**
    create m n_e-dimension particles and initialize velocity and position for the particle i
  end for
  repeat
    for each particle i **do**
      update the velocity and position of particle i within the velocity limitation $[V_{min}, V_{max}]$
      calculate the distance L_k though $f(x)$ of particle i;
    end for
    for each particle i **do**
      update the best position of particle i
      update the best position of the whole swarm
    end for
  until END_CONDITION
end procedure

Algorithm 3 GA for Bead Trapping Selection

Input: $f(x)$: cost funtion; p_b: position of all beads in field; n_e: number of electrodes; n_b: number of beads;
Output: optimal $x^* \in p_b$

procedure MAIN
  label the beads p_b with integral number
  encode the beads into chromosomes
  randomly generate m initial individuals
  repeat
    generate new population by crossover and mutation with the probabilities of crossover P_{cro} and mutation P_{mu}
    calculate the distance L_k though $f(x)$ of each individual;
    replace the low-distance individuals in the old generation with the high-distance individuals in the new generation
  until END_CONDITION
  Decode the chromosomes into the beads
end procedure

the image were labeled with an integral number. With nine electrodes on the microchip, numerous artificial particles with 9-D vectors were randomly placed within a field with different velocities. In each iteration, the positions and velocities of the particles were updated and the total moving distances were calculated. The best positions for each particle and the entire swarm were recorded for the next iteration. A summary of the pseudocode is shown in Algorithm 2. The number of the swarm m is $30 \times n_b$. The velocity range is set between $V_{\min} = -0.9 \times n_b$ (lower bound) and $V_{\max} = 0.9 \times n_b$ (upper bound). The number of generations is 3000.

D. Genetic Algorithm (GA)

GA is a metaheuristic method inspired by the process of natural selection, in which the best individuals are selected for the reproduction of the next generation. This approach belongs to the class of a random-based evolutionary algorithm and commonly used to generate high-quality solutions for optimization and search problems by performing three bio-inspired operations, namely, mutation, crossover, and selection. This algorithm repeatedly modifies a population of individual solutions. Each solution has a chromosome containing the features that define an individual and a fitness value that represent the quality of the solution. The beads for patterning are labeled with integral numbers and encoded into the chromosomes. In each iteration, the chromosomes are processed with crossover, mutation, and selection to generate a new population. The total moving distances for each individual are calculated to ensure that the low-distance individuals in the new generation will be selected to replace the high-distance individuals in the old generation. Finally, the generation will leave the individuals with good performance and the best one will be selected and decoded. A summary of the pseudocode is presented in Algorithm 3. The number of individuals m is $100 \times n_b$. The initial population size is randomly selected and roulette selection is used for chromosome selection. The probabilities for crossover P_{cro} and the mutation rate P_{mu}

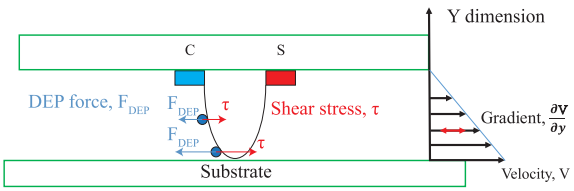

Fig. 10. Force analysis of the PS beads in the system.

are 0.8 and 0.3, respectively. Mutation of real-valued population is used for chromosome mutation and multiple-point crossover is used for recombination. The number of generations is set to 200.

V. Results and Discussion

Simulations and experiments were conducted to examine the performance of the system for single-bead patterning. First, the selection of the platform velocity in the bead trapping efficiency was tested. Since a PID controller was used to enhance the microbead for path following, the accuracy of the final bead position with and without PID control was also investigated. To find the most suitable optimization algorithm for high-efficiency PS bead patterning, different methods, including DFS, were first simulated under various conditions, including different numbers of PS beads and electrodes. On the basis of the results, the best optimization strategy was selected and adopted in the system. Different PS bead patterns were constructed on a glass substrate to demonstrate the feasibility and performance of the system. Finally, the system was tested with different size microparticles to show its robustness.

A. Selection in the Stage Velocity

A PS bead is subjected to drag force while moving it in an aqueous environment. During patterning, the micromanipulation system introduced a relative motion between the microchip and substrate. As the substrate moves at velocity V, it will create a motion in the fluid that follows a linear velocity profile along with the channel height, h, as shown in Fig. 10. At the boundary, the induced shear stress (τ) acted equally with and oppositely from the fluid and substrate, with the following differential relation:

$$\tau = \mu \frac{\partial V}{\partial y} \tag{7}$$

where μ is the viscosity of the medium.

To hold the PS beads firmly, the shear force acting on the beads must be equal to or less than the n-DEP force generated from the microchip ($\tau \leq F_{\mathrm{DEP}}$). Therefore, the maximum velocity of the stage must satisfy the following equation:

$$M \frac{V_{\max}}{h}(2\pi r^2) = 2\pi r^3 \varepsilon_m \cdot \mathrm{Re}[K(\omega)] \cdot \nabla E^2 \tag{8}$$

$$V_{\max} = rh\varepsilon_m \cdot \mathrm{Re}[K(\omega)] \cdot \nabla E^2 / M \tag{9}$$

where M is mass of the particle and $2\pi r^2$ is the surface area of the half-spherical object.

According to (9), if the height and medium electrical properties are known, then the maximum velocity becomes directly related to the square of the strength gradient of the electric field. In the microchip simulation [shown in Fig. 1(b)], the strength of the electric field was dependent on the distance with respect to the electrode center and voltage input. Given that the bead position could change over time, directly deriving the maximum velocity from the equation would be difficult. To find a suitable stage moving velocity in a given voltage input, the relationship between the stage moving velocity and the input signal voltage was explored through experiments. First, a voltage was supplied to hold a bead on a substrate, and the substrate on the stage began to move at an increasing speed until the bead slides away.

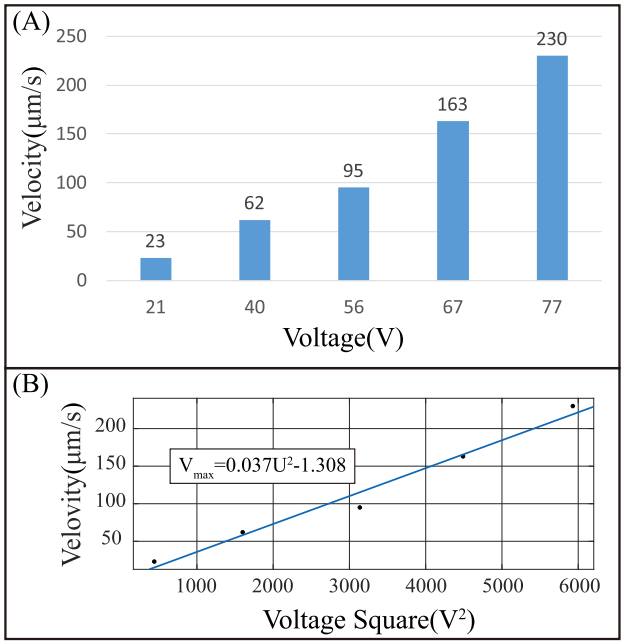

Fig. 11. (a) Maximum moving speed with different input signal voltages. (b) Relationship between the maximum velocity and voltage square.

The corresponding maximum velocity was recorded, and the results using different voltages are shown in Fig. 11(a). The results confirmed that as the voltage increases, a higher stage velocity can be used. The relationship between velocity and voltage input approximately followed the theoretical correlation, as derived from (9) [shown in Fig. 11(b)]. Based on the results, a high-voltage input should be selected, allowing the stage to move at the maximum speed and reduce the patterning time. However, if the voltage is too high, it could lead to a potential short circuit due to a dielectric breakdown. In this work, the maximum stage velocity was set to 20 μm/s where the voltage input was set to at least 20 V to prevent the beads from slipping away from the electric field.

B. Single-Bead Patterning

To perform bead separation between two nearby beads successfully, one of the beads must be positioned precisely within the electrode. The PID controller was used to guide the bead to the desired position, and the parameters used in the PID controller were as follows: control gain $K_p = 0.6$, $K_i = 0$, and $K_d = 0.001$, and time constant $T_f = 0.2$ s.

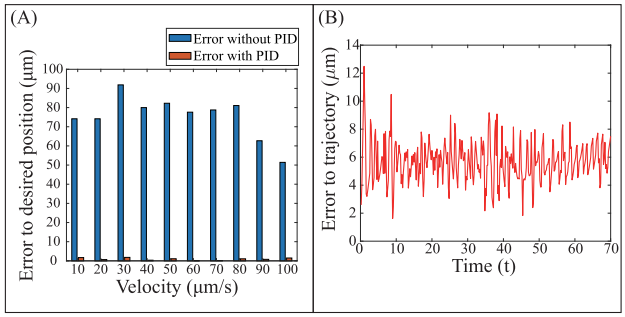

Fig. 12. (a) Error of the desired position with different velocities. (b) Tracking performance in a curved path.

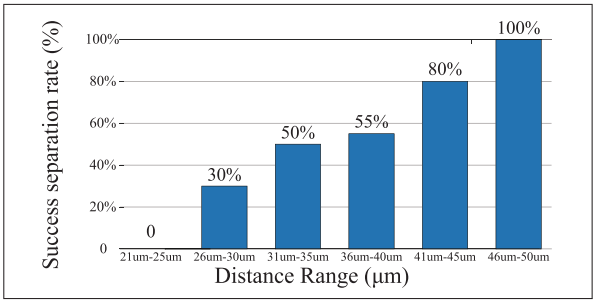

Fig. 13. Success rate of bead separation at the different bead distances.

Fig. 12(a) shows that the absence of a PID controller in the manipulation of beads obtained a position error of around 80 μm even if the velocity of the platform was set to 100 μm/s. This large error was mainly due to the shift or displacement between the bead and substrate during movement. The error can be reduced to almost zero with the implementation of PID control and tracking. Fig. 12(b) shows the performance of the PID controller in tracking a curve path with the platform moving at 20 μm/s. The bead could efficiently follow the desired path with an average error of 5 μm throughout the tracking.

Bead separation was then performed after the bead reached the desired position. Beads at random positions were grouped in pairs, and the performance in bead separation is shown in Fig. 13. The initial distance between the two beads would strongly influence the success rate of bead separation. If the two beads have already adhered together, the two beads would become inseparable, act as a single entity, and would be induced only one net dipole. In the beads that are sufficiently close, the interference from the beads would alter the electric field distribution near the boundary of the electrode and cause a shift in the crossover point (sign change in the DEP force) and direction of the net dipole induced on the beads (indirectly opposite to one another). The success rate of separation versus the different initial distances is shown in Fig. 13. A high success rate could be guaranteed if the initial distance between the beads was greater than 40 μm. This condition could be satisfied when a low-concentration PS bead solution was used in the experiments.

C. Optimization Algorithm Simulation

To examine the performance of the four optimization algorithms, the algorithms were coded in MATLAB to perform simulations with a personal computer. Two important simulation parameters, the number of beads and the number of electrodes, were adjusted. In the first set, the number of electrodes was set to 4×4, and the beads increased from 2^4 to 2^{10} [see Fig. 14(a)–(c)]. In the second set, the electrode number increased from 2×2 to 8×8 [see Fig. 14(d)–(f)]. The simulations were normalized to simplify the procedure. The positions of the electrodes were first set through the number of array electrodes and distributed in a 1-by-1 square. The beads were then randomly distributed. The cost function was calculated on the basis of the positions of electrodes and beads. The bead positions were updated accordingly after each step. The performance of optimization algorithms was analyzed on three aspects: the computational time to find the solution [Fig. 14(a) and (d)], the total distance traveled by the stage [Fig. 14(b) and (e)], and the total time used to move particles into respective electrodes, that is, the sum of the first two results [Fig. 14(c) and (f)]. The results in Fig. 14(a) and (d) show that increasing the number of particles or electrodes will lead to a significant increase in computational time in all the global optimization algorithms (ACO, PSO, and GA). PSO would take the longest time to find the solution, whereas DFS was the fastest method. In terms of the total distance traveled, Fig. 14(b) shows that if the number of particles available for patterning is small, the global optimization methods show better performance than the local optimization method. However, when more particles were available, the optimality of the solution found in GA and PSO was not guaranteed. Only ACO could still find the best solution (shortest distance) among the methods. Similar results were also observed in Fig. 14(e). When additional electrodes were used for trapping, ACO could still find the shortest distance but not in GA or PSO. The results also align with general findings on different optimization methods. PSO is considered because of its advantages of easy implementation and effectiveness for optimizing a wide range of functions [33]. GA is preferred for handling a small population. For a large population, the global update approach in ACO will outperform other methods, with the higher efficiency to converge to the best solution [34].

As the simulation on the distance traveled was normalized according to the electrode numbers, to calculate the total time needed to complete the entire procedure with an $N \times N$ electrode array, the total time T_t can be expressed as follows:

$$T_t = T_c + \frac{L_{\min}}{V} \times \frac{d_e}{1/(N+1)} \tag{10}$$

where T_c is the computational time, $L_{\min}$ is the total moving distance, V is the velocity of the platform, which is equal to 20, and d_e is the distance between the adjacent electrodes, which is equal to 1400 μm. After conversion and calculation, the total time, including the computation time and time required to move the stage, is plotted in Fig. 14(c) and (f). Similar results were found as the simulation results of Fig. 14(b) and (e). The findings indicated that the performance of the optimization result played a leading role in the total

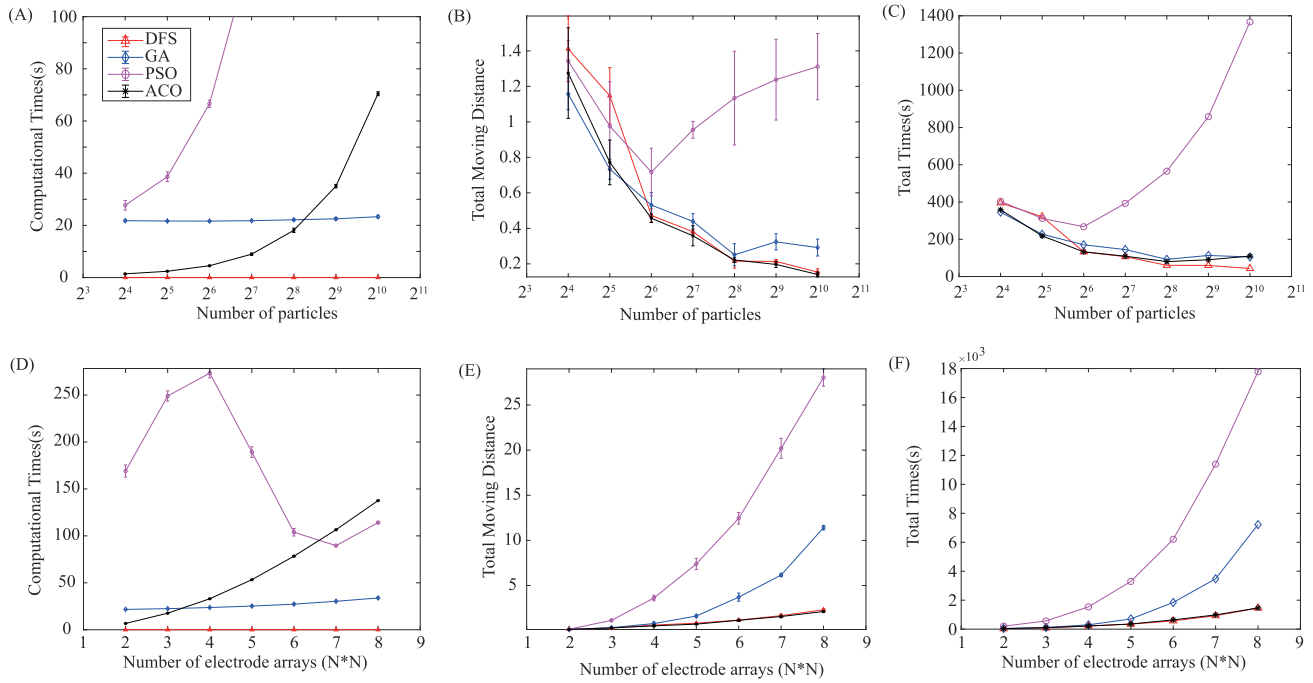

Fig. 14. Time and performance simulation of various algorithms in different situations. (a)–(c) Simulation with different numbers of particles. (d)–(f) Simulation with different numbers of electrode arrays ($N \times N$). (a) and (d) Computational time. (b) and (e) Total moving distance for patterning. (c) and (f) Total time used to complete the entire process.

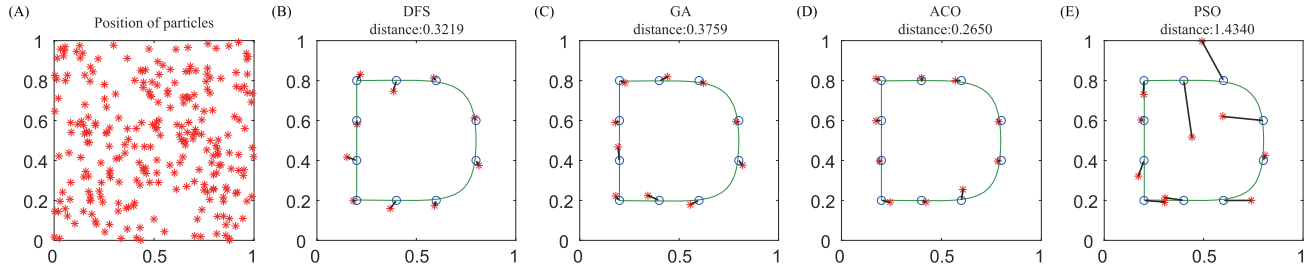

Fig. 15. Patterning simulation of various algorithms in the character "D" by using a 4×4 electrode array. (a) Position of the initial particle. Selective particles and their translation routes after each step with (b) DFS, (c) GA, (d) ACO, and (e) PSO.

time consumed in the entire procedure. For example, although it would cost a significant amount of time to obtain the solution shown in Fig. 14(a) and (d), the optimality of the solution in the ACO algorithm could help to shorten the stage's required distance to travel and achieve the shortest time in completing the entire procedure [see Fig. 14(c) and (f)]. This phenomenon could be explained by (10). In a smaller velocity, the second part of (10) would be larger than the first part and dominate the equation. Hence, the application of the proper optimization method is important to achieve high efficiency in bead patterning and yield the optimal solution for bead selection.

To further compare the performance of the different algorithms, another simulation was conducted using a configuration with 2^8 beads [Fig. 15(a)] and a 4×4 electrode array. To form the pattern of the character "D," 10 out of 16 electrodes [black circles shown in Fig. 15(b)–(e)] were chosen as the target electrodes in the cost function. Red stars represented the bead, as selected from the algorithm after each step. The black lines indicated the distance that each bead needed to move, and the total distance was calculated and labeled in the figure. The simulation result also confirmed that ACO demonstrated the best performance among the four algorithms.

To further illustrate the concept of implementing the optimization algorithm for bead patterning, a simulation with a 4×20 electrode array was used to generate a series of characters. The results between ACO and DFS were compared. The initial positions of the different beads are shown in Fig. 16(a). The chosen electrodes were indicated in blue circles, while the beads selected via ACO and DFS were exhibited with black stars and purple crosses, respectively [see Fig. 16(b)]. The simulation result showed that the ACO optimization method offered a better result than the DFS with a large number of array electrodes.

D. Verification of the Automatic Patterning Program

The performance of the micropatterning system with the implementation of the ACO algorithm was examined experimentally. The PS beads in the AHA solution were used to

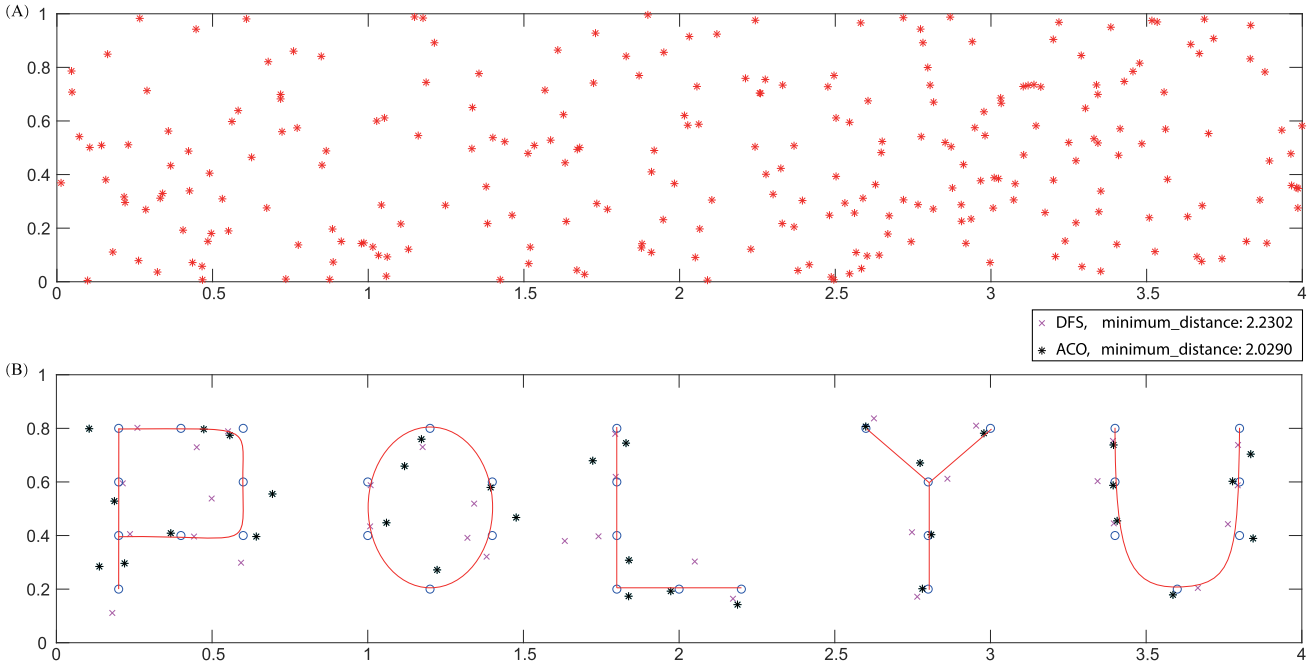

Fig. 16. Patterning simulation between DFS and ACO with a series character "POLYU" by a 4×20 electrode array. (a) Position of initial particle. (b) Selective particles after each step with DFS and ACO.

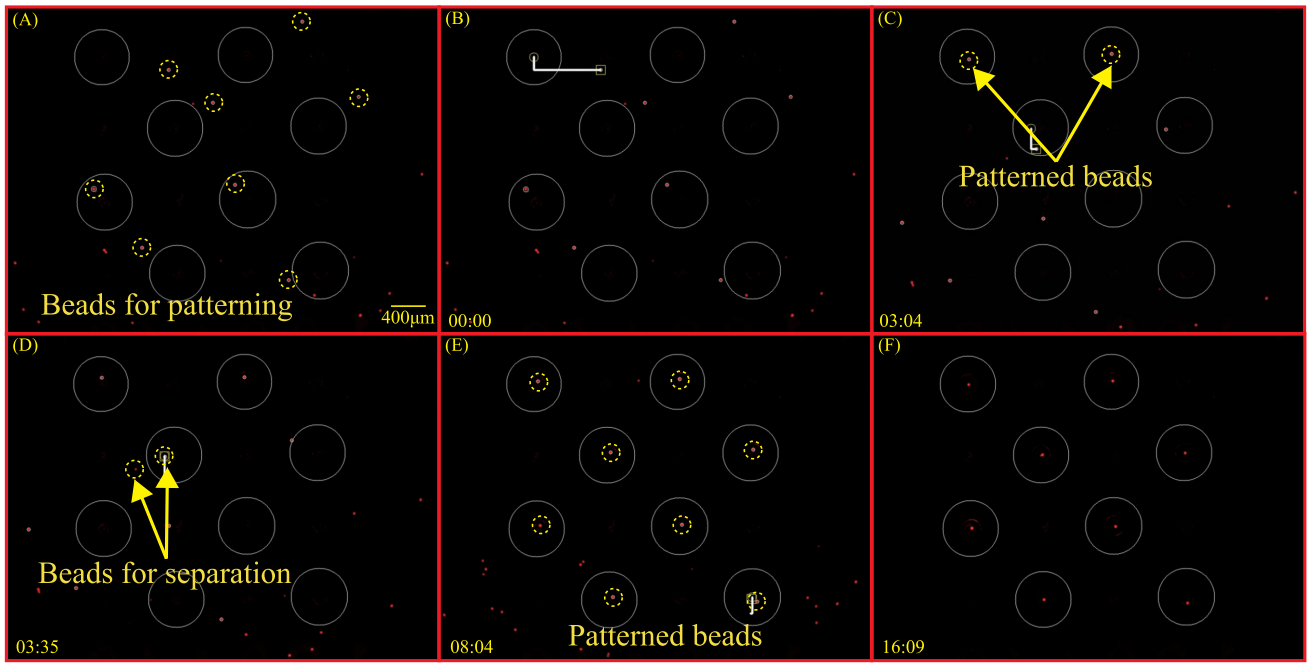

Fig. 17. Automatic patterning procedure of eight PS beads with divided form. Eight single 40-μm beads can be patterned sequentially underneath the desired electrodes (white circles).

create patterns on the glass substrate, as shown in Fig. 17. The position information of PS beads was evaluated in the beginning. Based on the bead separation algorithm, the optimal trapping position in each bead was calculated and recorded. In any bead that cannot guarantee the successful implementation of single-bead trapping, its information would be removed and excluded in the optimization algorithm for calculation. The remaining bead information was proceeded by the ACO algorithm to find the optimal path in patterning. The electrode positions were highlighted in white circles, whereas the beads selected by the algorithm were demonstrated in yellow circles [see Fig. 17(a)]. The beads were then transferred to the center of the electrodes sequentially along with the path created for the PID following [Fig. 17(b)]. The corresponding electrode was switched on to hold the bead [shown in Fig. 17(c)]. In case the bead needs to be separated before trapping,

the bead was directed to the specific position as obtained from the separation algorithm [see Fig. 17(d)]. By following the procedure, multiple PS beads were successfully trapped using the selected electrodes [see Fig. 17(e)] and the bead pattern was transferred to a clean area for the removal of the surrounding abundant beads [see Fig. 17(f)].

VI. Conclusion

The scarcity of cell samples and high cost associated with drugs led to the large demand for accurate single-cell patterning. In this study, an electrode array microchip with a design of 4×4 dot electrodes was combined with the micromanipulation system to construct single-bead patterns efficiently. Micro PS beads were selected for patterning on the glass substrate, which was controlled through the motorized platform of the microscope. Image processing techniques were used to extract information for position evaluation and automatic bead selection. By controlling the relay, the specific electrode can be energized and trap the beads, forming different single-microparticles patterns. The PID controller was adopted to guide the bead to follow the desired path. To avoid multiple beads from being trapped in one electrode, a bead separation method was proposed on the basis of the electric field distribution at the electrode boundary. To find the minimum patterning time, the problem statement in patterning was described and solved using different global optimization methods (ACO, PSO, and GA). Although simulations showed that GA and PSO are not effective for finding the optimal solution in a large population, ACO can always achieve the best performance. This finding indicated that the solution from DFS is suboptimal, compared with the best solution found in the global optimization method. The ACO algorithm was implemented in the system. The experiments confirmed that the system could successfully pattern the PS beads on the substrate. The adhesion force might cause failure when large beads were used. Based on the findings, the proposed system with the ACO algorithm could provide a low-cost, flexible, and effective method using nDEP to create the single-bead pattern for cell-based assays and characterization. This microchip can also be easily adjusted according to the application. Compared with conventional LOC devices, separating the microchip with electrodes from the LOC device increases the flexibility of the system and enables precise control and selective trapping for single-particle patterning.

References

[1] T. Yasukawa, "Rapid and simple immunoassay based on negative dielectrophoresis with three-dimensional interdigitated array electrodes," *ECS Trans.*, vol. 50, no. 12, p. 139, 2013.

[2] J. Zhou *et al.*, "High-content single-cell analysis on-chip using a laser microarray scanner," *Lab Chip*, vol. 12, no. 23, pp. 5025–5033, 2012.

[3] C. E. Sims and N. L. Allbritton, "Analysis of single mammalian cells on-chip," *Lab Chip*, vol. 7, no. 4, pp. 423–440, 2007.

[4] G. Kim, S.-J. Yeom, S.-C. Jang, C.-S. Lee, C. Roh, and H.-H. Jeong, "Simple analysis of lipid inhibition activity on an adipocyte micro-cell pattern chip," *Biomolecules*, vol. 8, no. 2, p. 37, Jun. 2018.

[5] Z.-B. Liu, Y. Zhang, J.-J. Yu, A. F.-T. Mak, Y. Li, and M. Yang, "A microfluidic chip with poly(ethylene glycol) hydrogel microarray on nanoporous alumina membrane for cell patterning and drug testing," *Sens. Actuators B, Chem.*, vol. 143, no. 2, pp. 776–783, Jan. 2010.

[6] H. A. Pohl, *Dielectrophoresis: The Behavior of Neutral Matter in Nonuniform Electric Fields*. Cambridge, U.K.: Cambridge Univ. Press, 1978.

[7] K. Ino *et al.*, "Manipulation of microparticles for construction of array patterns by negative dielectrophoresis using multilayered array and grid electrodes," *Biotechnol. Bioeng.*, vol. 104, no. 4, pp. 709–718, 2009.

[8] B. Yafouz *et al.*, "The design and simulation of a planar microarray dot electrode for a dielectrophoretic lab-on-chip device," *Int. J. Electrochem. Sci.*, vol. 7, no. 12, pp. 12054–12063, 2012.

[9] N. Manaresi *et al.*, "A CMOS chip for individual cell manipulation and detection," in *IEEE Int. Solid-State Circuits Conf. (ISSCC) Dig. Tech. Papers*, Dec. 2003, pp. 192–487.

[10] P. Y. Chiou, A. T. Ohta, and M. C. Wu, "Massively parallel manipulation of single cells and microparticles using optical images," *Nature*, vol. 436, no. 7049, pp. 370–372, Jul. 2005.

[11] S. Zhang *et al.*, "Patterned optoelectronic tweezers: A new scheme for selecting, moving, and storing dielectric particles and cells," *Small*, vol. 14, no. 45, Nov. 2018, Art. no. 1803342.

[12] Y. Yang, Y. Mao, K.-S. Shin, C. O. Chui, and P.-Y. Chiou, "Self-locking optoelectronic tweezers for single-cell and microparticle manipulation across a large area in high conductivity media," *Sci. Rep.*, vol. 6, no. 1, Sep. 2016, Art. no. 22630.

[13] S. Zhang *et al.*, "Assembly of topographical micropatterns with opto-electronic tweezers," *Adv. Opt. Mater.*, vol. 7, no. 20, Oct. 2019, Art. no. 1900669.

[14] M. Grad, A. W. Bigelow, G. Garty, D. Attinger, and D. J. Brenner, "Optofluidic cell manipulation for a biological microbeam," *Rev. Sci. Instrum.*, vol. 84, no. 1, Jan. 2013, Art. no. 014301.

[15] K.-W. Huang *et al.*, "Microfluidic integrated optoelectronic tweezers for single-cell preparation and analysis," *Lab Chip*, vol. 13, no. 18, pp. 3721–3727, 2013.

[16] L. Miccio, V. Marchesano, M. Mugnano, S. Grilli, and P. Ferraro, "Light induced DEP for immobilizing and orienting escherichia coli bacteria," *Opt. Lasers Eng.*, vol. 76, pp. 34–39, Jan. 2016.

[17] S. Chowdhury *et al.*, "Automated cell transport in optical tweezers-assisted microfluidic chambers," *IEEE Trans. Autom. Sci. Eng.*, vol. 10, no. 4, pp. 980–989, Oct. 2013.

[18] S. Chowdhury, A. Thakur, P. Svec, C. Wang, W. Losert, and S. K. Gupta, "Automated manipulation of biological cells using gripper formations controlled by optical tweezers," *IEEE Trans. Autom. Sci. Eng.*, vol. 11, no. 2, pp. 338–347, Apr. 2014.

[19] A. G. Banerjee, A. Pomerance, W. Losert, and S. K. Gupta, "Developing a stochastic dynamic programming framework for optical tweezer-based automated particle transport operations," *IEEE Trans. Autom. Sci. Eng.*, vol. 7, no. 2, pp. 218–227, Apr. 2010.

[20] A. G. Banerjee, S. Chowdhury, W. Losert, and S. K. Gupta, "Real-time path planning for coordinated transport of multiple particles using optical tweezers," *IEEE Trans. Autom. Sci. Eng.*, vol. 9, no. 4, pp. 669–678, Oct. 2012.

[21] T. Ju, S. Liu, J. Yang, and D. Sun, "Rapidly exploring random tree algorithm-based path planning for robot-aided optical manipulation of biological cells," *IEEE Trans. Autom. Sci. Eng.*, vol. 11, no. 3, pp. 649–657, Jul. 2014.

[22] H. Yang, X. Li, Y. Liu, and D. Sun, "Automated transportation of biological cells for multiple processing steps in cell surgery," *IEEE Trans. Autom. Sci. Eng.*, vol. 14, no. 4, pp. 1712–1721, Oct. 2017.

[23] X. Li, C. C. Cheah, S. Hu, and D. Sun, "Dynamic trapping and manipulation of biological cells with optical tweezers," *Automatica*, vol. 49, no. 6, pp. 1614–1625, Jun. 2013.

[24] C. C. Cheah, X. Li, X. Yan, and D. Sun, "Observer-based optical manipulation of biological cells with robotic tweezers," *IEEE Trans. Robot.*, vol. 30, no. 1, pp. 68–80, Feb. 2014.

[25] X. Li and C. C. Cheah, "Tracking control for optical manipulation with adaptation of trapping stiffness," *IEEE Trans. Control Syst. Technol.*, vol. 24, no. 4, pp. 1432–1440, Jul. 2016.

[26] X. Li and C. C. Cheah, "A simple trapping and manipulation method of biological cell using robot-assisted optical tweezers: Singular perturbation approach," *IEEE Trans. Ind. Electron.*, vol. 64, no. 2, pp. 1656–1663, Feb. 2017.

[27] K. Huang, H. K. Chu, B. Lu, and L. Cheng, "Characterization of a microchip device for cell patterning via negative dielectrophoresis," in *Proc. IEEE Int. Conf. Robot. Biomimetics (ROBIO)*, Dec. 2018, pp. 1521–1526.

[28] K. Huang, B. Lu, J. Lai, and H. K. H. Chu, "Microchip system for patterning cells on different substrates via negative dielectrophoresis," *IEEE Trans. Biomed. Circuits Syst.*, vol. 13, no. 5, pp. 1063–1074, Oct. 2019.

[29] K. Huang, H. K. Chu, B. Lu, J. Lai, and L. Cheng, "Automated cell patterning system with a microchip using dielectrophoresis," in *Proc. Int. Conf. Robot. Autom. (ICRA)*, May 2019, pp. 634–639.
[30] K. Huang, Z. Cui, I. A. Ajamieh, J. Lai, J. K. Mills, and H. K. Chu, "Automated single-microparticle patterning system for micro-analytics," in *Proc. IEEE 16th Int. Conf. Autom. Sci. Eng. (CASE)*, Aug. 2020, pp. 390–396.
[31] S. Suzuki and K. Be, "Topological structural analysis of digitized binary images by border following," *Comput. Vis., Graph., Image Process.*, vol. 30, no. 1, pp. 32–46, Apr. 1985.
[32] S. Hu and D. Sun, "Automatic transportation of biological cells with a robot-tweezer manipulation system," *Int. J. Robot. Res.*, vol. 30, no. 14, pp. 1681–1694, 2011.
[33] M. N. Ab Wahab, S. Nefti-Meziani, and A. Atyabi, "A comprehensive review of swarm optimization algorithms," *PLoS ONE*, vol. 10, no. 5, May 2015, Art. no. e0122827.
[34] S. Sivanandam and S. Deepa, "Genetic algorithms," in *Introduction to Genetic Algorithms*. Berlin, Germany: Springer, 2008, pp. 15–37.

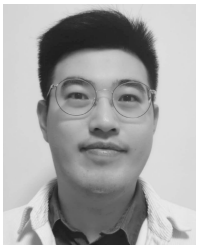

Kaicheng Huang received the B.Eng. degree from the Department of Automation from Shenzhen University, Shenzhen, Guangdong, China, in 2014, the M.Sc. degree in mechanical and automation engineering from The Chinese University of Hong Kong, Hong Kong, in 2015, and the Ph.D. degree in mechanical engineering from the Hong Kong Polytechnic University, Hong Kong, in 2020.

He is currently a Postdoctoral Fellow with the Department of Industrial and Manufacturing Systems Engineering, The University of Hong Kong, Hong Kong. His current research interests include micromanipulation and nanomanipulation and automation.

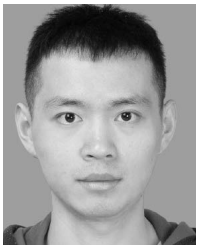

Zhenxi Cui received the B.Eng. degree from the Department of Mechanical Engineering, Shandong University of Technology, Shandong, China, in 2014, and the M.Sc. degree from the Department of Mechanical Engineering, The Hong Kong Polytechnic University, Hong Kong, in 2016, where he is currently pursuing the Ph.D. degree.

His current research interests are robotic cooperative control, deformable object manipulation, and trajectory plan.

Jiewen Lai (Student Member, IEEE) received the B.Eng. degree in metallurgical engineering from the Wuhan University of Science and Technology, Wuhan, China, in 2016, and the M.Sc. degree in mechanical and automation engineering from The Chinese University of Hong Kong, Hong Kong, in 2017. He is currently pursuing the Ph.D. degree in mechanical engineering with The Hong Kong Polytechnic University, Hong Kong.

His research interests include soft/continuum robots and surgical robots.

Bo Lu received the B.Eng. degree from the Department of Ship and Offshore Engineering, Dalian University of Technology, Liaoning, China, in 2013, the M.S. degree (Hons.) and Ph.D. degrees from the Department of Mechanical Engineering, The Hong Kong Polytechnic University, Hong Kong, in 2015 and 2019, respectively.

He is currently a Postdoctoral Research Fellow with the T Stone Robotics Institute, The Chinese University of Hong Kong, N.T., Hong Kong. His current research interests include medical robotics, computer vision, vision-based manipulation and intervention.

Henry K. Chu (Member, IEEE) received the B.A.Sc. degree in mechanical engineering from the University of Waterloo, Waterloo, ON, Canada, in 2005, and the M.Sc. and Ph.D. degrees in mechanical and industrial engineering from the University of Toronto, ON, Canada, in 2007 and 2011, respectively.

He was a Postdoctoral Fellow with the University of Toronto and The City University of Hong Kong, Hong Kong. He is currently an Assistant Professor with The Hong Kong Polytechnic University, Hong Kong. His research interests include robotic manipulation, vision-based control and automation, microsystem design, and tissue engineering.